



## Journal of Advanced Research in Fluid Mechanics and Thermal Sciences

Journal homepage:  
[https://semarakilmu.com.my/journals/index.php/fluid\\_mechanics\\_thermal\\_sciences/index](https://semarakilmu.com.my/journals/index.php/fluid_mechanics_thermal_sciences/index)  
ISSN: 2289-7879



# Laboratory-Scale Low-Speed Water Tunnel: Comparison of Experimental Flow Visualization and Computer-Aided Simulation

Fredy Surahmanto<sup>1,\*</sup>, Dipta Adityantoro<sup>2</sup>, Adi Ridwan Satria<sup>2</sup>

<sup>1</sup> Department of Mechanical Engineering Education, Universitas Negeri Yogyakarta, Indonesia

<sup>2</sup> Applied Undergraduate Program of Mechanical Engineering, Universitas Negeri Yogyakarta, Indonesia

### ARTICLE INFO

#### Article history:

Received 22 February 2023

Received in revised form 30 May 2023

Accepted 6 June 2023

Available online 22 June 2023

#### Keywords:

Computational fluid dynamics; flow visualization; simulation; water tunnel

### ABSTRACT

This study aimed at developing the laboratory-scale low-speed water tunnel design by first evaluating the effect of varying the number of wide-angle diffuser vanes and then confirming flow visualization against object geometries tested by experiments and computer-aided simulation. The low-speed water tunnel design in this study consists of a wide-angle diffuser, a honeycomb, a convergent section, and a working section. To ascertain the laminar flow of water would act in the experiment, a prior simulation using 3, 6, and 12 vanes and without a vane was conducted. Some geometries, including tube, triangle, aerofoil, and car models have been tested and then compared to the experimental results. The results indicate that the twelve vanes diffuser is more effective in minimizing turbulent flow and producing a streamlined pattern in the water tunnel. Laminar flow with a Reynolds number of 2238 and flow velocity of 0.008 m/s was obtained in the working section. The flow visualization by experiment and computational fluid dynamics simulation was almost similar.

## 1. Introduction

A water tunnel is an experimental facility used to test the aerodynamic and hydrodynamic behaviour of submerged objects in flowing water. This test is almost the same as a wind tunnel, but there are differences in the fluid, namely using water as a working fluid, and the phenomena being investigated such as measuring the strength of lift or drag and flow patterns on an object [1-3]. Water tunnels are sometimes used instead of wind tunnels to take measurements such as particle image velocimetry (PIV) because they are easier to implement in water. Particle image velocimetry (PIV) is a method used to visualize a fluid flow using a photo technique [4,5]. In a wind tunnel, the propulsion is usually a multi-blade propeller with an adjustable blade pitch, while in a water tunnel, a pump is used as fluid propulsion. Moreover, a water tunnel model can be built at a lower price than a wind tunnel [6].

\* Corresponding author.

E-mail address: [fredy\\_surahmanto@uny.ac.id](mailto:fredy_surahmanto@uny.ac.id)

<https://doi.org/10.37934/arfmts.107.1.142164>

Fluid behavior in a stationary or moving state and the effects caused by these fluids are studied by fluid mechanics. Fluid can be defined as a substance whose shape can change continuously due to shear forces. Shear force is a component of the force offending the surface. A fluid that is rest means that there is no shear stress at all [7]. The application of the principles of fluid mechanics can be found in everyday life as well as in industry.

To identify the type of flow that occurs in the water tunnel, the Reynolds number is used. The Reynolds number is the ratio of inertia forces to viscosity [8]. As has been known that it is a parameter in determining the flow regime whether it is laminar or turbulent. As long as the Reynolds number is appropriate, the results are valid. The desired flow regime can be achieved by conditioning the flow channel, wherein the water tunnel equipment usually comprises a wide-angle diffuser, settling chamber, contraction, and working section.

Analysis to get a visualization of the flow on an object by conventional or experimental means has limitations related to the accuracy of the data obtained. In addition, the experimental method has difficulties in setting up the test section and requires a large enough space and high operational costs. In general, water tunnels are used in the commercial industry for research purposes and are built to a very large size. For example, Rolling Hills Research Corporation's model 1520 water tunnel requires a laboratory space of 10 m x 5 m x 2 m (length x width x height) containing 3785 liters of water and speeds varying from 0 m/s - 0.6 m/s with a manufacturing cost of hundreds of thousands of USD [9]. The use of computational methods with sufficient accuracy can complement the experimental method [10]. By using a computer system, the operating costs will be less, and the geometry can be freely reproduced to the actual size without having to physically construct the geometry.

Research related to water tunnel has been conducted are very limited. Sargison *et al.*, [11] researched the design and calibration of water tunnels for boundary layer research of an object. The water tunnel in this study consists of several parts, namely a wide-angle diffuser, settling chamber, contraction, and working section with a size of 2400 x 200 x 600 mm. The total dimensions of the water tunnel are 8 m long, 2 m wide, and 2.3 m high. The flow velocity in this water tunnel reaches 2 m/s. In this research, there are variations in the number of diffuser vanes, namely 3 and 6 diffuser vanes, each of which was carried out by CFD simulation. The results of this research show that the number of 6 diffuser vanes will minimize the turbulence that occurs in the water tunnel so that the best results of the boundary layer of an object can be achieved.

Another research on the design, fabrication and analysis of low-speed water tunnel was carried out by Kalgutkar *et al.*, [12]. Unlike the former, the water tunnel in this study was designed without a diffuser with a working section size of 70 x 10 x 15 cm. The flow velocity in this water tunnel is 0 m/s to 0.2 m/s. There are 4 objects in this study, namely the shape of the tube, NACA 2412 airfoil, triangle shape, and nozzle. This study compares the flow visualization in CFD with the experimental flow visualization. This study shows that the experimental flow visualization was almost similar to the CFD flow visualization. Based on that research, it is challenging to assure laminar flow takes place in the working section by designing the appropriate wide-angle diffuser.

It is known that a broad variety of scientific instruments are offered commercially. The equipment becomes unusable after only a few years due to the high cost of these systems and the scarcity of spare components [13]. Meanwhile, building a large water tunnel would require high costs and large space. Thus, it is urgent to make a water tunnel with low cost and acceptable quality for research and educational purposes. Therefore, this study aimed to develop a laboratory-scale low-speed water tunnel design by evaluating the number of wide-angle diffuser vanes to gain laminar flow in the working section and confirming flow visualization by experiment and computer-aided simulation to prove that the fabricated water tunnel is representative for research as well as teaching purpose.

## 2. Methodology

As shown in Figure 1, the water tunnel design in this study consists of several main parts, namely the wide-angle diffuser, honeycomb, convergent section, and working section. Several geometries of test objects, namely tube, triangle, airfoil, and car model, were used. Observations were made to compare the flow patterns between those obtained by CFD simulation and by experiments on the test objects.

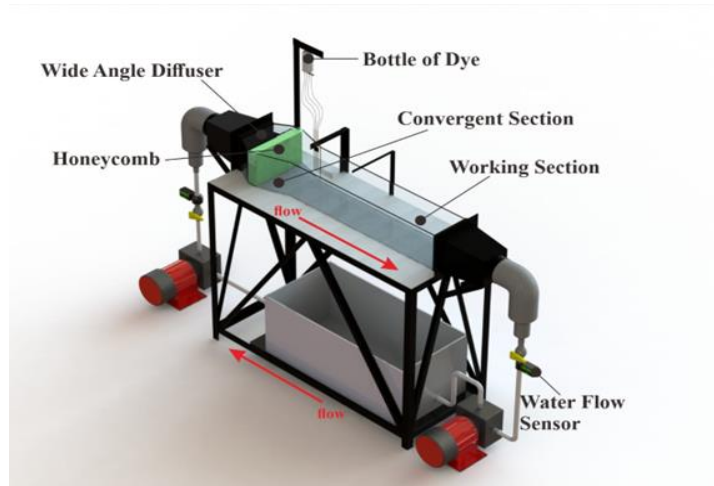


Fig. 1. Isometric drawing of low-speed water tunnel design

### 2.1 Working Section

The working section design is in the form of a block of 1.25 m x 0.25 m x 0.25 m in size. The inlet and outlet sections are squares of 0.25 m x 0.25 m in size. This working section functions as a place for experimental flow visualization of the test object.

### 2.2 Convergent Section

The convergent section is a space for the converging plane to continue and accelerate the flow out of the honeycomb to the working section. A well-designed convergent section will accelerate the flow, reduce turbulence intensity, and create uniform flow [14]. In this study, the convergent section has an inlet area of 0.4 m x 0.25 m, an outlet area of 0.25 m x 0.25 m, and a length of 0.3 m with a convergent plane angle of 35°.

### 2.3 Honeycomb

A honeycomb is a part used to minimize turbulent flow. Honeycombs are not included in the diffuser performance CFD model, but their presence is expected to improve diffuser stability and performance [15]. The main purpose of the honeycomb is to straighten the flow by reducing speed. Honeycomb resistance also improves flow uniformity and reduces the rate of flow turbulence [16]. The honeycomb length is 5 to 10 times the diameter of the space cells, and optimal results will be obtained if the honeycomb has 25,000 space cells [17]. The honeycomb must be located in front of the convergent section so that the flow in the testing section will be laminar [14]. The honeycomb design in this study as shown in Figure 2 has a size of 0.4 m x 0.25 m x 0.06 m and a diameter of 0.006

m with plastic material. The honeycomb length is 10 times the cell diameter. This honeycomb is placed before the convergent section.

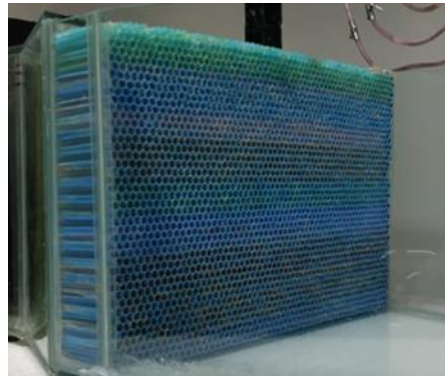


Fig. 2. Honeycomb

### 2.4 Wide Angle Diffuser

Wide-angle diffusers are designed with internal vanes to minimize turbulence in the flow and to provide a stable flow [18]. The ratio of the area from the inlet to the outlet at the wide-angle diffuser should be less than 2.5 cm and the vane angle ratio should be  $5^{\circ}$ - $7^{\circ}$  to control the flow separation [19]. Various studies using simulations have been carried out to prove that the computational fluid dynamics simulation method can be used as an approach to solving problems in research. Computational Fluid Dynamics (CFD) is a method for converting fluid dynamics control equations in the form of integrals and derivatives into discretized algebraic form, which can be solved by a computer to obtain the values of the flow field at a specific discrete point or time [20]. CFD plays an important role in understanding and analyzing complex flow patterns [21]. In this study, as shown in Figure 3, the wide-angle diffuser design used an inlet size of 0.25 m x 0.25 m and an outlet of 0.4 m x 0.25 m. The ratio of the inlet and outlet area is 1.6 cm. Several variations in the number of vanes at the wide-angle diffuser were 0 vanes, 3 vanes, 6 vanes, and 12 vanes with a vane angle ratio of  $5^{\circ}$  and  $10^{\circ}$  and a vane thickness of 3 mm. This study selected the number of vanes with the best internal flow by testing several geometric objects using the Computational Fluid Dynamics (CFD) method.

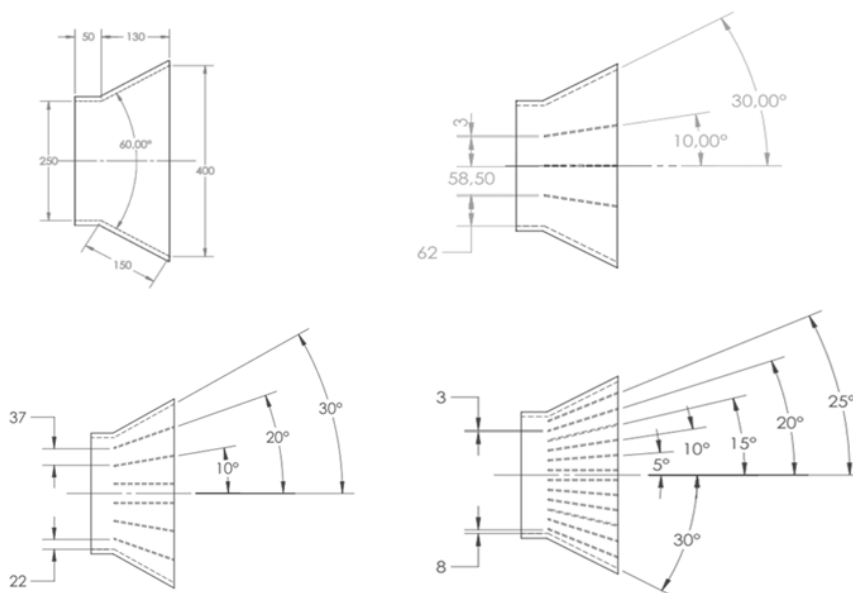
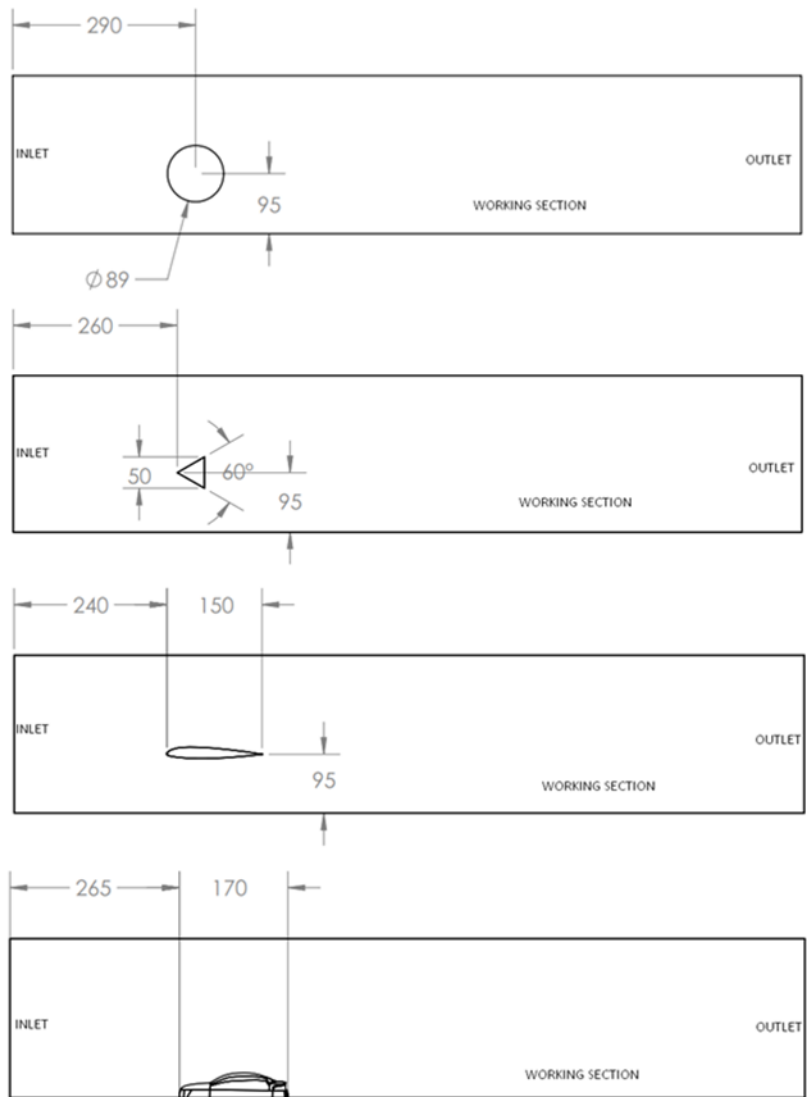


Fig. 3. Design of wide-angle diffuser without and with 3, 6, 12 vanes

## 2.5 Geometry Object

In this study four geometry objects were tested for flow simulation in the water tunnel geometry with the best number of diffuser vanes, these objects are tube geometry, triangle, airfoil, and sedan type car. Each geometry object was placed in the working section. The simulation results of the geometry object were compared with the experimental results of the test object in the water tunnel. Figure 4 is a picture of the dimensions of the location of the geometry that will be tested in the water tunnel.



**Fig. 4.** Location of the Geometry Objects: tube, triangle, airfoil, and sedan-type car

## 2.6 Simulation

### 2.6.1 Geometry of the water tunnel model

The water tunnel geometry model was created using Solid Works software and then exported to Ansys Fluent in IGS format. This model has undergone simplification in its creation to facilitate the meshing process in the simulation. This simplification includes only making the fluid domain geometry. There were variations in the number of diffuser vanes that were added to the wide-angle

diffuser in the water tunnel. Figure 5 is an image of the geometry of the water tunnel model with a variation in the number of diffuser vanes.

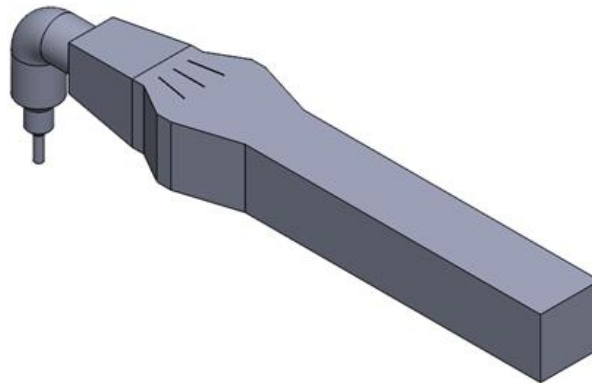


**Fig. 5.** Geometry of the water tunnel model

### 2.6.2 Meshing

The meshing process in this study was carried out using the automatic meshing method and used a tetrahedron mesh shape. Meshing is the process of discretising a continuous fluid domain into a discrete computational domain so that the equations in it can be solved and a solution produced. The tighter the meshing elements, the more thorough the simulation process. If the meshing process is successful, it can be continued to the setup and boundary condition process, but if there are still errors in the mesh, the meshing process should be repeated, or the water tunnel design should be improved. Table 1 is the detail of mesh settings on the water tunnel geometry. Figure 6 is the result of meshing the water tunnel geometry.

**Table 1**  
Detail of mesh

Sizing	Size Function	Curvature
	Relevance Center	Coarse
	Mesh Defeaturing	Yes (Default)
	Transition	Slow (Default)
Body Sizing	Element Size	8 mm
	Size Function	Uniform
	Behaviour	Hard
Statistics	Elements	2210980

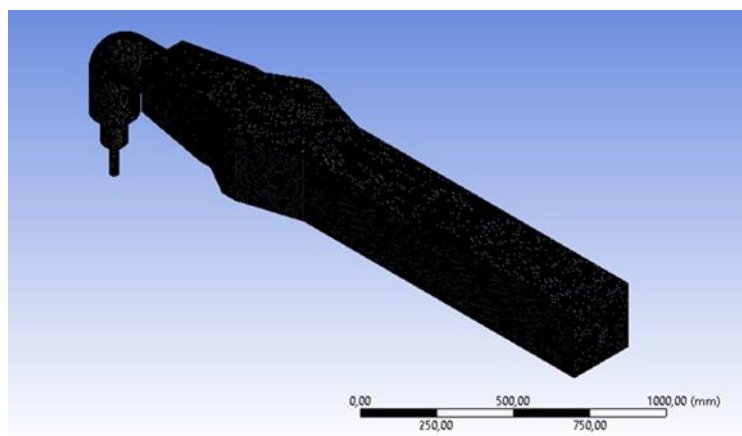


**Fig. 6.** Result of meshing

### 2.6.3 Setting setup and boundary condition

After that, in the setup settings, the flow method and material to be used were selected. Boundary conditions are specified at the inlet, outlet, and object. The residual convergence criteria for the iteration process were following the default criteria in ANSYS Fluent, namely with a residual value of  $1 \times 10^{-5}$  and an iteration value of 1000 times. If the iteration has not reached convergence, the meshing obtained is not appropriate and must iterate again. Computation was performed in ANSYS Fluent with input setup settings in Table 2 and input solution in Table 3.

**Table 2**  
ANSYS Fluent simulation setup setting

General	Solver Type	Pressure-Based
	Time	Steady
	Velocity Formulation	Absolute
	Gravity	9.81 m/s <sup>2</sup>
Models	Energy	off
	Viscous Model	K-epsilon (2 eqn)
Material	Fluid	Water Liquid
Boundary Condition	Inlet	Velocity Inlet (Magnitude)
		0.5 m/s
	Outlet	Outflow

**Table 3**  
ANSYS Fluent simulation solution setting

Methods	Scheme	SIMPLE
	Gradient	Least Squares Cell-Based
	Pressure	Second Order
	Momentum	Second Order Upwind
	Turbulent Kinetic Energy	Second Order Upwind
	Turbulent Dissipation Rate	Second Order Upwind
Monitors	Residual	1e-05 (All Absolute Criteria)
Initialization	Initialization Methods	Standard Initialization
	Compute from	All-zones
Run Calculation	Number of Iterations	1000

## 2.7 Theoretical Basics

### 2.7.1 Laminar and turbulent flow

The transition from laminar flow to turbulent flow depends on geometry, surface roughness, flow velocity, surface temperature, and fluid type, among others. The Reynolds number is used to identify the type of flow that occurs. Reynolds number is the ratio of inertial forces to viscous force [8]. For flow in a pipe, the Reynolds number can be formulated as Eq. (1)

$$Re = \frac{V \cdot D}{\nu} \tag{1}$$

where  $V$  is average flow velocity (m/s<sup>2</sup>),  $\nu$  is kinematic viscosity (m<sup>2</sup>/s), and  $D$  is hydraulic diameter (m). Under most practical conditions, the flow in a circular pipe is laminar for  $Re \leq 2300$ , turbulent for  $Re \geq 4000$ , and transitional in between.

### 2.7.2 Conservation of mass principle

The conservation of mass principle for a control volume can be expressed as the net mass transfer to or from a control volume during a time interval  $\Delta t$  is equal to the net change (increase or decrease) in the total mass within the control volume during  $\Delta t$ . The continuity equation results from the law of conservation of mass which states that the amount of mass of a substance is constant, so it can be written through the equation Eq. (1) [8]

$$A_1 V_1 = A_2 V_2 \quad (2)$$

where  $A_1, A_2$  is flow cross-section ( $m^2$ ) and  $V_1, V_2$  is average flow velocity (m/s).

### 2.7.3 Bernoulli equation

Bernoulli's equation for fluid flow is derived from the principle of energy conservation. The total energy in a fluid element consists of potential energy ( $E_p$ ), kinetic energy ( $E_k$ ), and flow energy. If no energy is added or there is no leakage between 2 points of a fluid flow, then Bernoulli's equation can be written as Eq. 3 [8]

$$Z_1 - Z_2 + \frac{V_1^2 - V_2^2}{2g} + \frac{P_1 - P_2}{\gamma} = 0 \quad (3)$$

where  $Z_1, Z_2$  is elevation head (m),  $V_1, V_2$  is fluid flow velocity (m/s),  $g$  is gravity acceleration ( $9.81 \text{ m/s}^2$ ),  $P$  is pressure ( $\text{N/m}^2$ ), and  $\gamma$  is specific gravity of fluid ( $\text{N/m}^3$ ).

### 2.7.4 Linear momentum equation

The general form of the linear momentum equation that applies to fixed, moving, or deforming control volumes is obtained according to Eq. (4) [8]

$$\sum \vec{F} = \frac{d}{dt} \int_{CV} \rho \vec{V} dV + \int_{CS} \rho \vec{V} (\vec{V}_r \cdot \vec{n}) dA \quad (4)$$

which can be stated as

$$\left( \begin{array}{l} \text{The sum of all} \\ \text{external forces} \\ \text{acting on a CV} \end{array} \right) = \left( \begin{array}{l} \text{The time rate of change} \\ \text{of the linear momentum} \\ \text{of the contents of the CV} \end{array} \right) + \left( \begin{array}{l} \text{The net flow rate of} \\ \text{linear momentum out of the} \\ \text{control surface by mass flow} \end{array} \right)$$

Here  $\vec{V}_r = \vec{V} - \vec{V}_{CS}$  is the fluid velocity relative to the control surface (for use in mass flow rate calculations at all locations where the fluid crosses the control surface), and  $\vec{V}$  is the fluid velocity as viewed from an inertial reference frame. The product  $\rho(\vec{V}_r \cdot \vec{n})$  represents the mass flow rate through area element  $dA$  into or out of the control volume.

### 2.8 Experimental Setup

The low-speed water tunnel design has a layout size of 3 m x 0.7 m x 2.8 m. The total volume of the low-speed water tunnel was 142 litres, and the water container volume was 210 litres. This

equipment used a pump as a booster for water flow with a pump output speed of 0.5 m/s. Figure 7 is a low-speed water tunnel equipment used in this study with detailed specifications as presented in Table 4. Objects and ink pipes were set as shown in Figure 8.

**Table 4**

The specification of low-speed water tunnel

Pump	Discharge (L)	22.54
	Outlet Velocity (m/s)	0.5
Wide-Angle Diffuser	Inlet area (cm <sup>2</sup> )	625
	Outlet area (cm <sup>2</sup> )	1000
	Ratio area	1.6
	Number of vanes diffuser	12
	Vane diffuser angle (°)	5
Honeycomb	Size (cm)	40 x 6 x 25
	Diameter Cell (mm)	6
Convergent Section	Inlet area (cm <sup>2</sup> )	1000
	Outlet area (cm <sup>2</sup> )	625
Working Section	Size (cm)	125 x 25 x 25
	Velocity Flow (m/s)	0.008
	Reynolds Number	2238

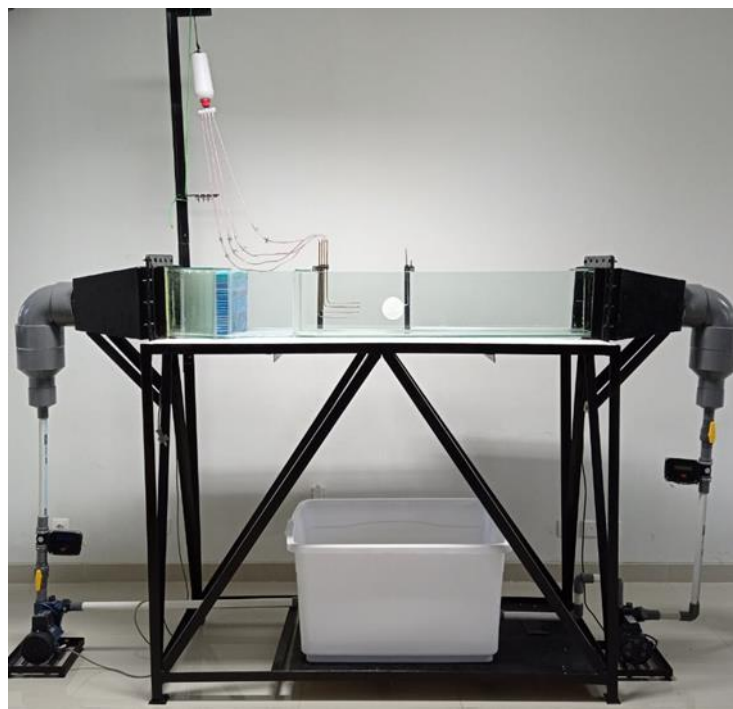


**Fig. 7.** Low-speed water tunnel equipment

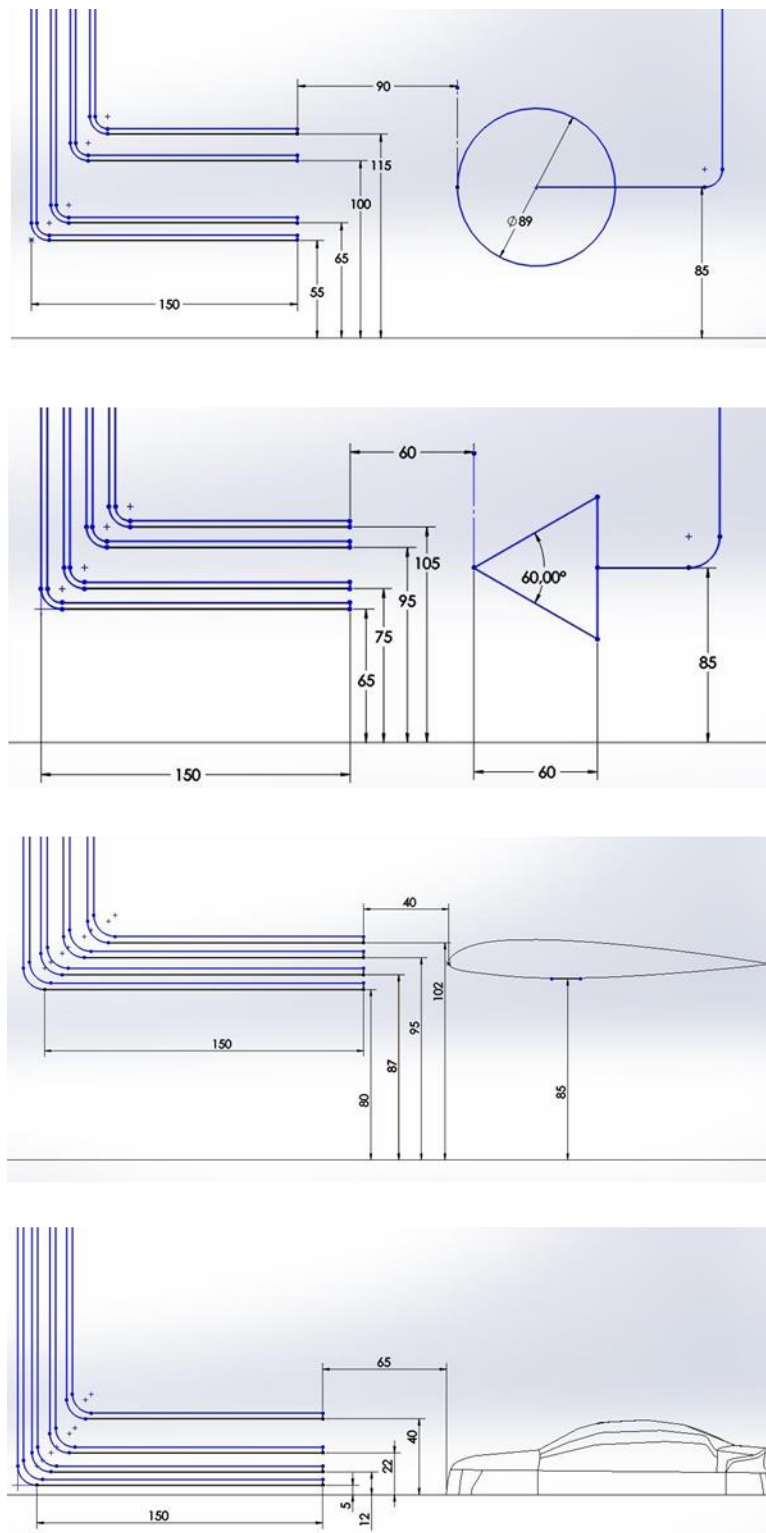


**Fig. 8.** Setting of ink pipes and the geometry objects: tube, triangle, airfoil, and car model

### 3. Results

#### 3.1 Analysis of Variation in the Number of Vanes on Wide Angle Diffuser

Visualization data in the form of streamlines on the wide-angle diffuser were collected by using ANSYS Results. The simulation was conducted to determine the number of diffuser vanes that would

be most effective to minimize the turbulent flow. The flow visualizations for each variation in the number of diffuser vanes are shown in Figure 9 to Figure 21.

Based on the visualisation of the water tunnel without a diffuser vane, much of unstable flows are flowing from the inlet to the convergent section as shown in Figure 9. In Figure 10, the red circle shows the occurrence of turbulent flow in the wide-angle diffuser to the convergent section. Figure 11 shows the percentage of turbulent intensity in the working section which is 0.16 %. Turbulent flow in the working section occurs because there are no components used to minimise turbulent flow from the pump outlet to the convergent section.

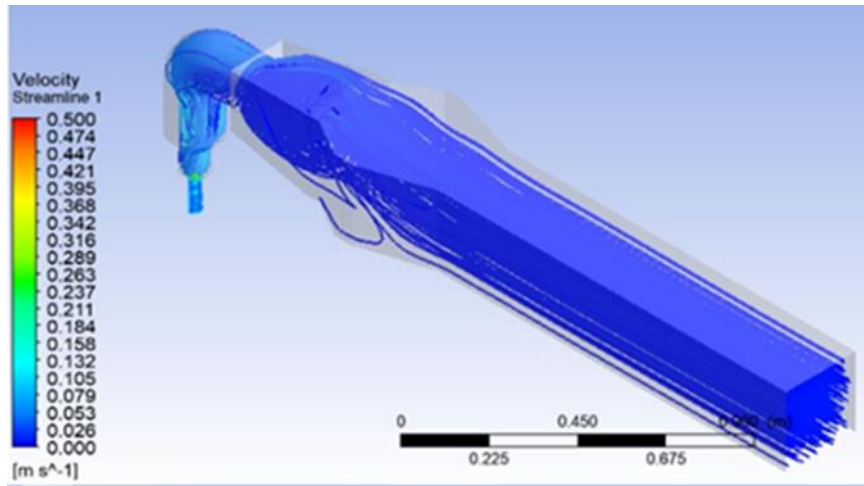


Fig. 9. Flow visualization without diffuser vane

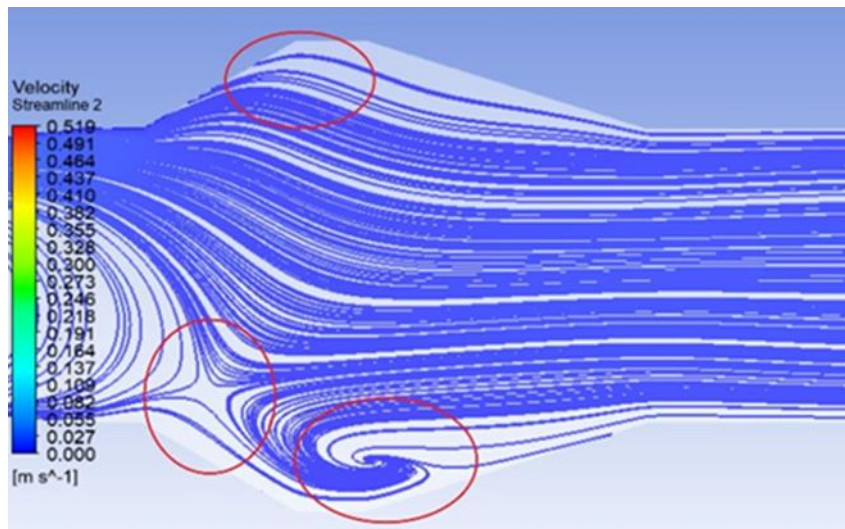


Fig. 10. Turbulent flow in wide angle diffuser without diffuser vane

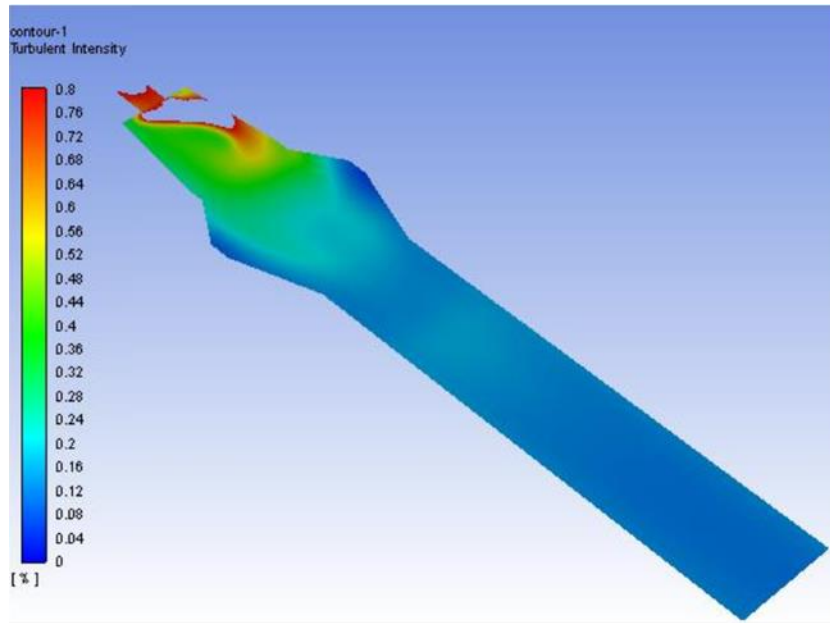


Fig. 11. Turbulent intensity contour without diffuser vane

The addition of multiple diffuser vanes was found to show a significant difference in flow shape than without using a vane diffuser. Based on the results of the three-vane diffuser flow visualisation as shown in Figure 12 and Figure 13, the addition of three diffuser vanes can minimise the turbulent flow that occurs in the wide-angle diffuser section to the convergent section, but the flow in the area is not yet fully laminar. In Figure 13, the red circle shows that there is still turbulent flow that occurs in the wide-angle diffuser area. Figure 14 shows the percentage of turbulent intensity in the water tunnel. The percentage of turbulent intensity in the working section is reduced to 0.12 % because there is a component to minimise turbulent flow that occurs in the wide-angle diffuser in the form of three diffuser vanes.

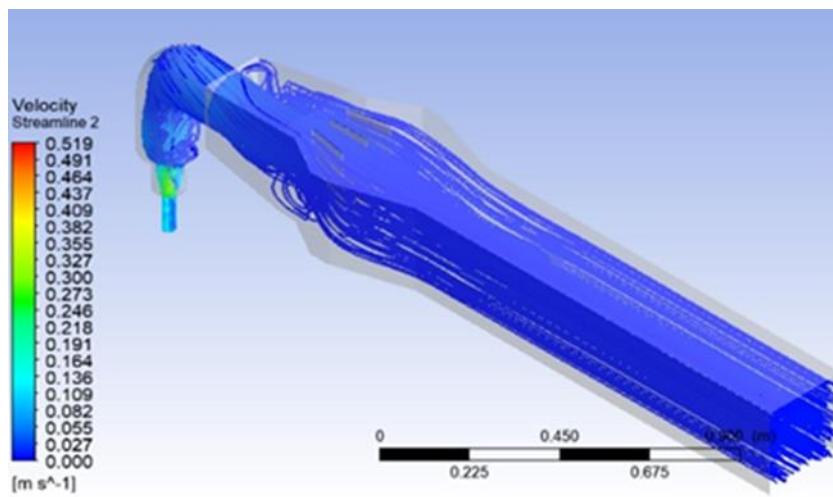
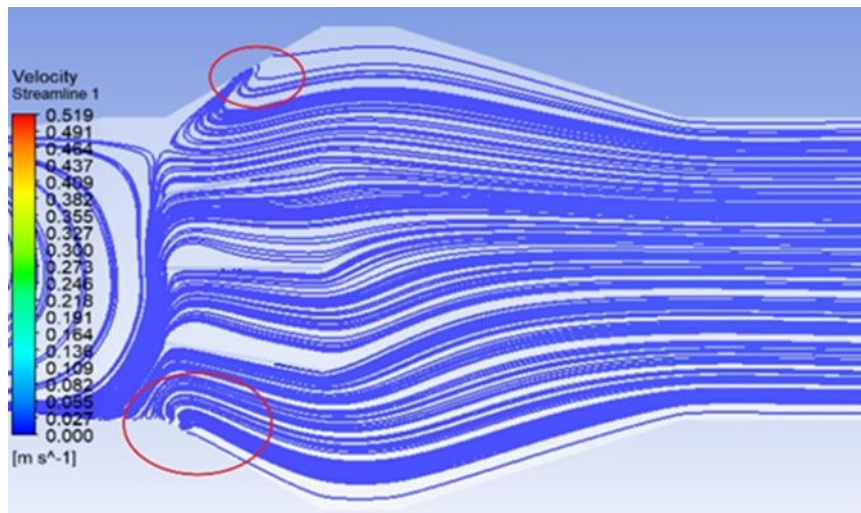
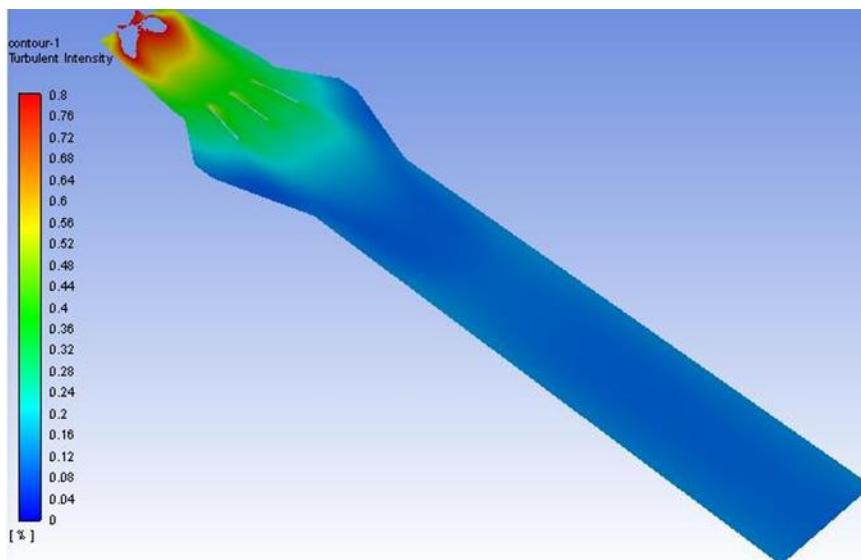


Fig. 12. Flow visualization with three diffuser vanes



**Fig. 13.** Turbulent flow in wide angle diffuser with three diffuser vanes



**Fig. 14.** Turbulent intensity contour with three diffuser vanes

The addition of six diffuser vanes resulted in the flow that is visualised in Figure 15. It gives the shape of the streamline pattern on the wide-angle diffuser to the convergent section, but there is still turbulence that occurs around the inlet section of the wide-angle diffuser as marked by the red circle in Figure 16. The addition of six diffuser vanes minimises the percentage of turbulent flow in the working section to 0.08 %, as shown in Figure 17. This result is rather different from that obtained by Sargison *et al.*, [11] that found stable and well behave flow.

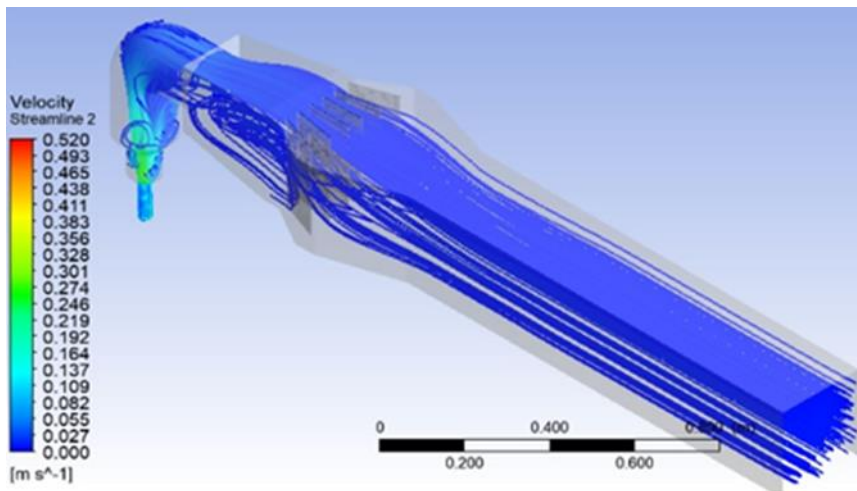


Fig. 15. Flow visualization with six diffuser vanes

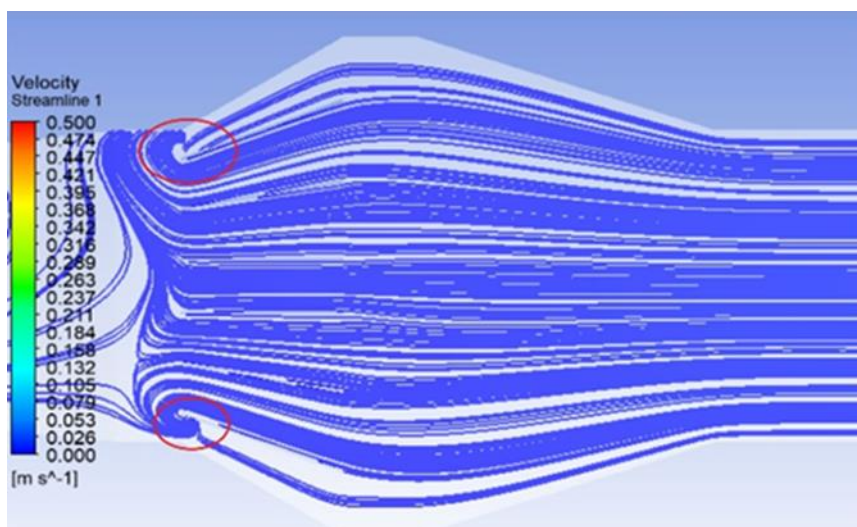


Fig. 16. Turbulent flow in wide angle diffuser with six diffuser vanes

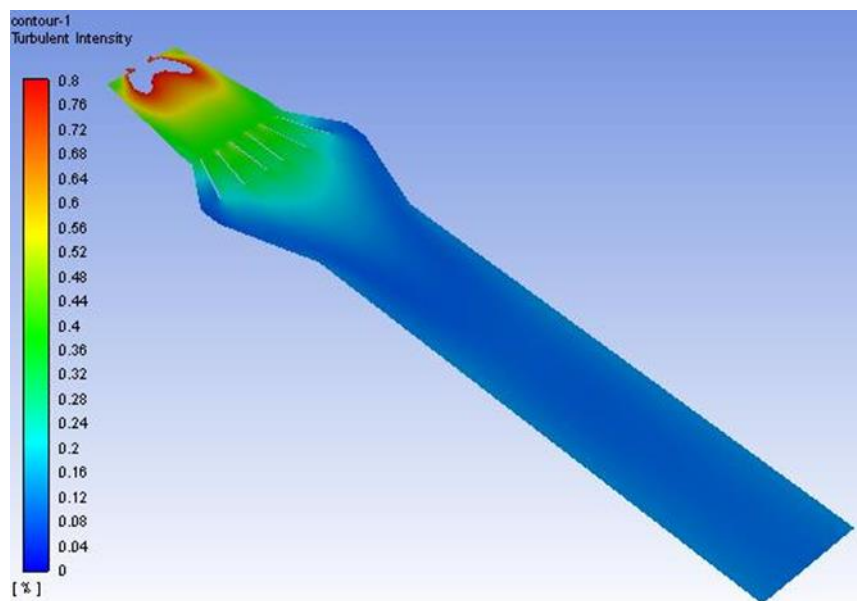


Fig. 17. Turbulent intensity contour with six diffuser vanes

From the visualisation shown in Figure 18, it can be observed that the addition of twelve diffuser vanes is the best variation in minimising the turbulent flow that occurs at the inlet of the wide-angle diffuser to the convergent section. The flow that flows in the area is evenly divided so that it forms a streamline pattern. Figure 19 shows that the flow from the wide-angle diffuser inlet to the working section forms a streamline pattern and no turbulent flow occurs. The addition of twelve diffuser vanes is also very effective in reducing the percentage of turbulent flow in the working section, which is 0.04 %. Figure 20 shows the percentage of turbulent intensity in the water tunnel with twelve diffuser vanes.

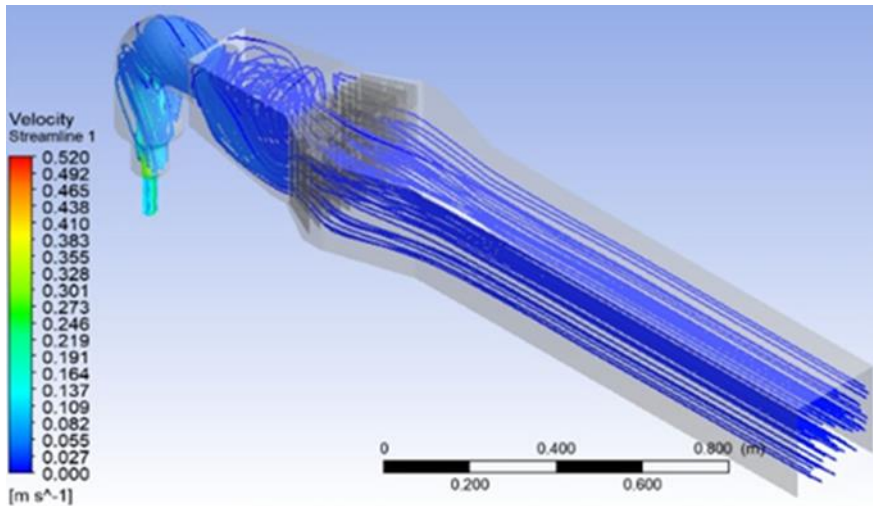


Fig. 18. Flow visualization with twelve diffuser vanes

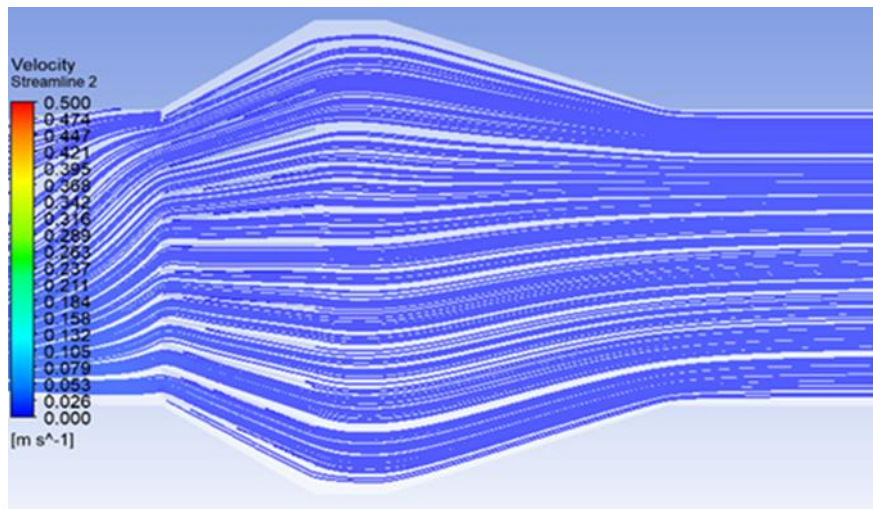
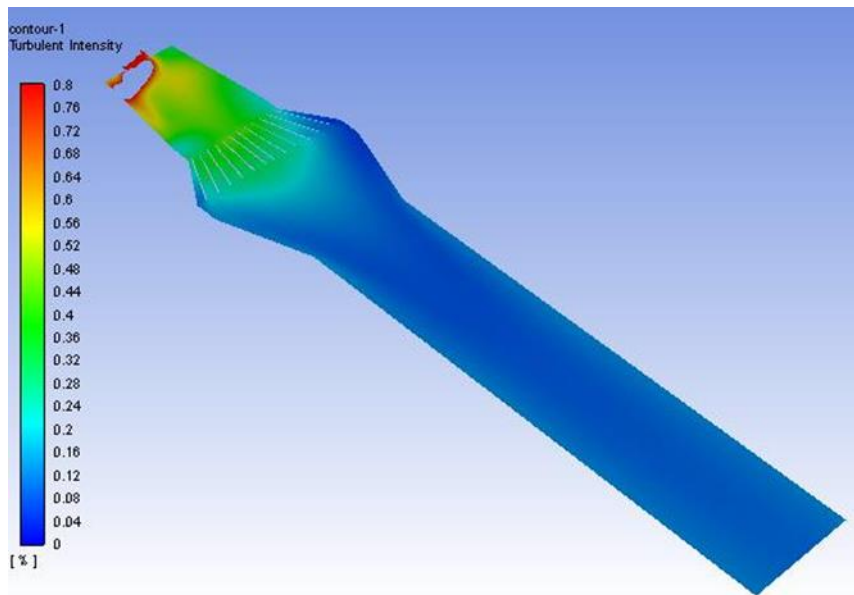


Fig. 19. Turbulent flow in wide angle diffuser with twelve diffuser vanes



**Fig. 20.** Turbulent intensity contour with twelve diffuser vanes

Based on the analysis above, it could be found that the twelve-vane diffuser with an angle ratio of  $5^\circ$  was the most effective variation to minimize the turbulent flow so it could be selected as the final design to be fabricated. With the twelve diffuser vanes, the percentage of turbulent flow in the working section which was originally 0.16 % can be minimised to 0.04 %.

Figure 21 is the top view of the velocity contour at the low-speed water tunnel. Once the speed of the working section is known, the Reynolds number can be calculated according to Eq. (1). The flow in the water tunnel formed a streamline pattern that encouraged flow visualization trials using several geometric objects.

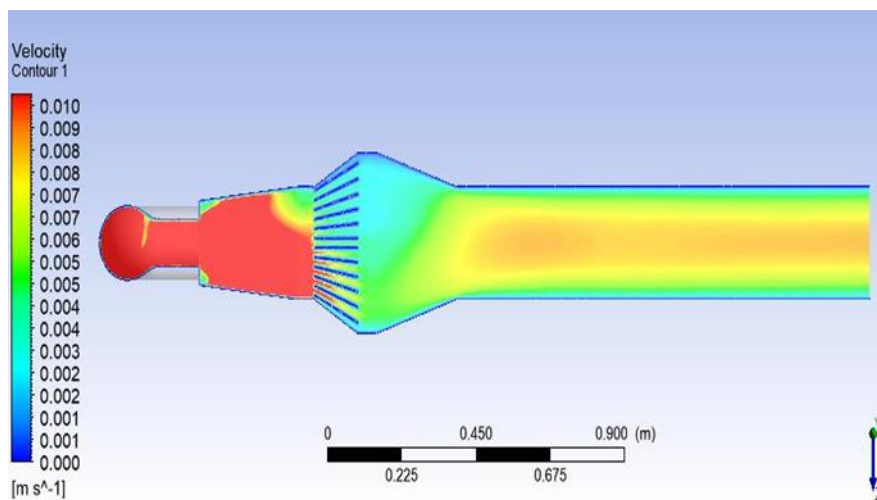


**Fig. 21.** Velocity contour low-speed water tunnel

### 3.2 Flow Visualization with Geometry Objects

In the present study, the flows around geometric objects such as a tube, triangle, airfoil, and car models were visualized and then compared to the experimental results.

### 3.2.1 Flow around tube

The comparison between experimental flow visualization and computer-aided simulation can be seen in Figure 22 and Figure 23. In these figures, the turbulent flow occurred in the area behind the tube.

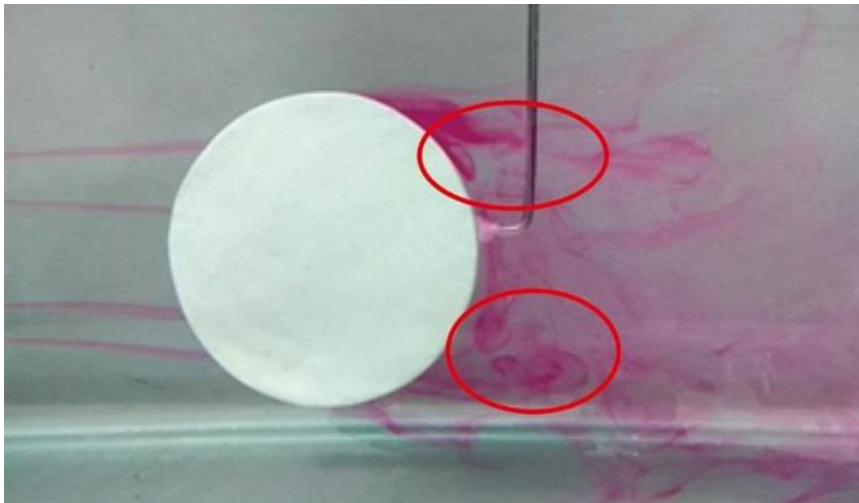


**Fig. 22.** Experimental flow visualization of a tube

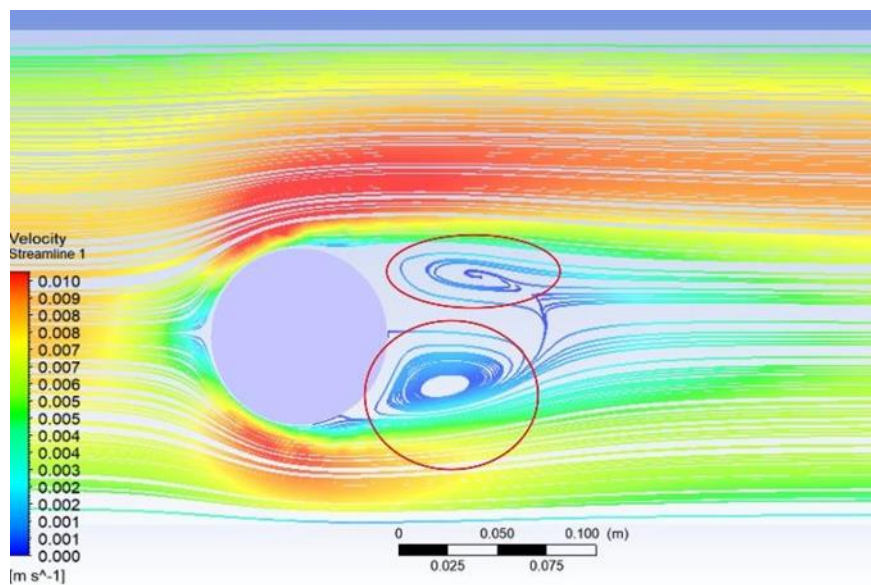


**Fig. 23.** Velocity streamlines of a tube by computer-aided simulation

Figure 24 shows that flow split when hitting the tube experienced an increase in speed (marked in red) and a decrease in speed after passing through the tube (marked in blue). The dark blue colour that surrounds the tube is the boundary layer effect, where there is flow friction with the surface of the object so that the flow velocity approaches 0 m/s. This phenomenon was in accordance with the previous research [22].

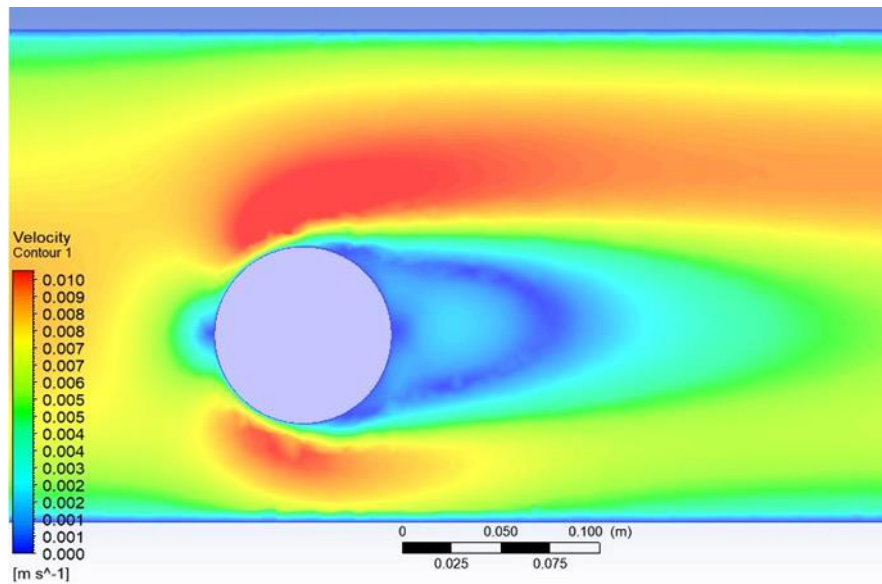


**Fig. 24.** Velocity contour of a tube by computer-aided simulation

### 3.2.2 Flow around triangle

Figure 25 and Figure 26 show the comparison between experimental flow visualisation and computer-aided simulation around a triangle, where turbulent flow also occurred in the area behind the triangle. As shown by Figure 27, the flow was split when passing through the triangle (marked in red) and underwent velocity increase, then decelerated after the triangle (marked in blue). This result was in line with the previous study [23].

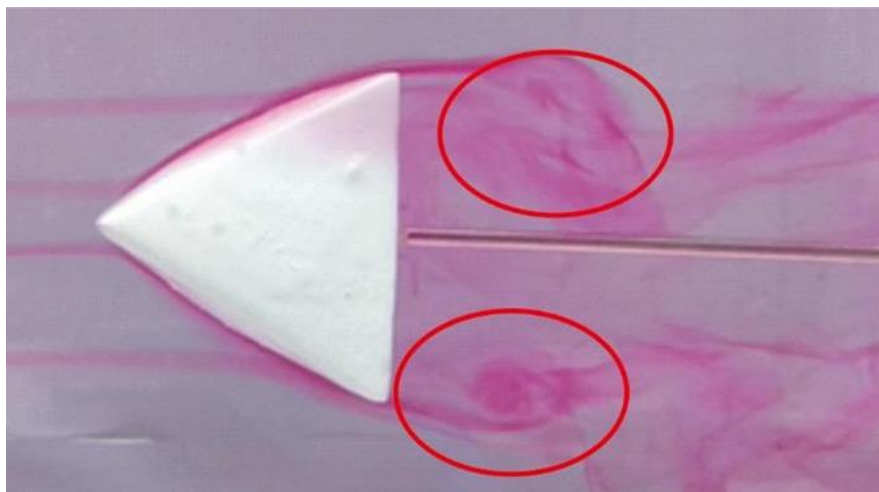


**Fig. 25.** Experimental flow visualization of a triangle

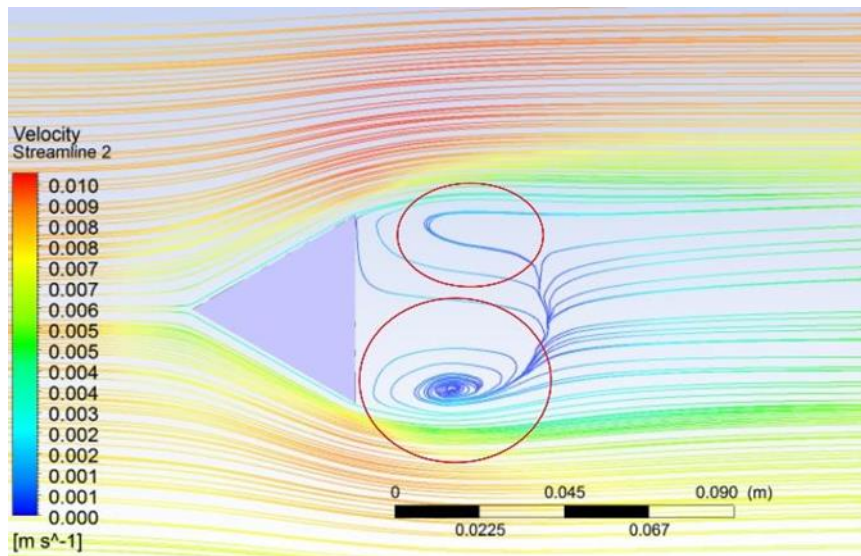


**Fig. 26.** Velocity streamline of a triangle by computer-aided simulation

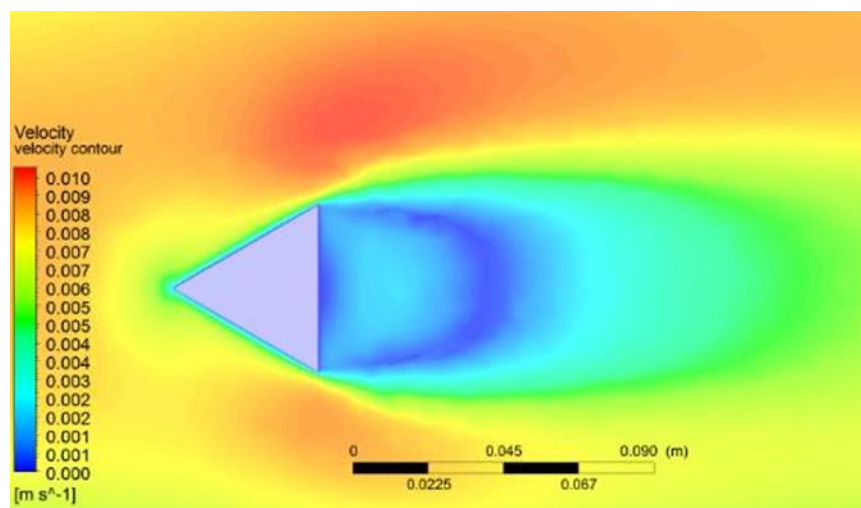


**Fig. 27.** Velocity contour of a triangle by computer-aided-simulation

### 3.2.3 Flow around airfoil

The comparison between experimental flow visualisation and computer-aided simulation around an airfoil can be seen in Figure 28 and Figure 29.

In Figure 28 and Figure 29, a streamline pattern occurred on the airfoil without turbulent flow. Figure 30 shows that the flow split when passing through an airfoil has an increase in speed (marked in red) and experienced a decrease in speed (marked in dark blue). The dark blue colour that surrounds the tube is the boundary layer effect, indicating that there was a flow friction with the surface of the object so that the flow velocity closed to 0 m/s. This result is in line with the previous study [24].

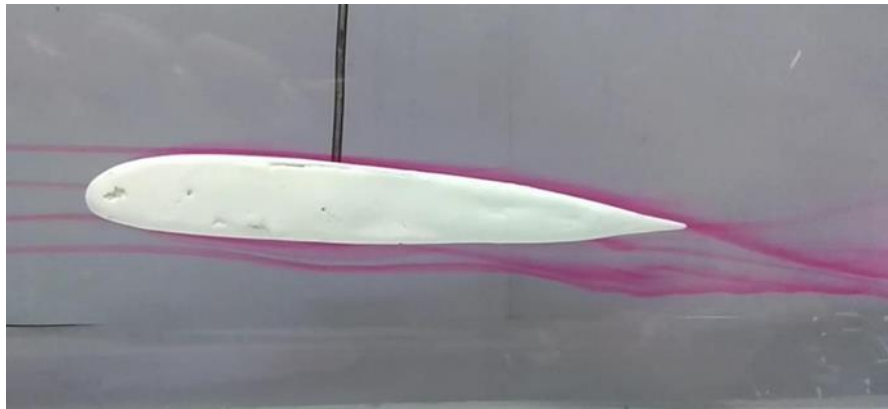


**Fig. 28.** Experimental flow visualization of an airfoil

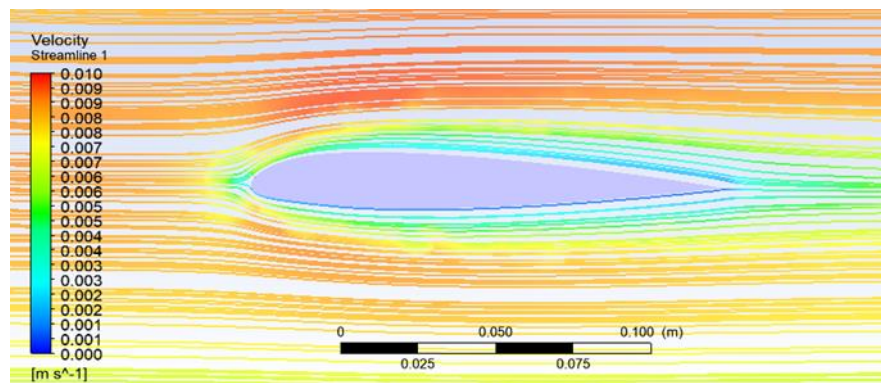


**Fig. 29.** Velocity streamlines of an airfoil by computer-aided simulation

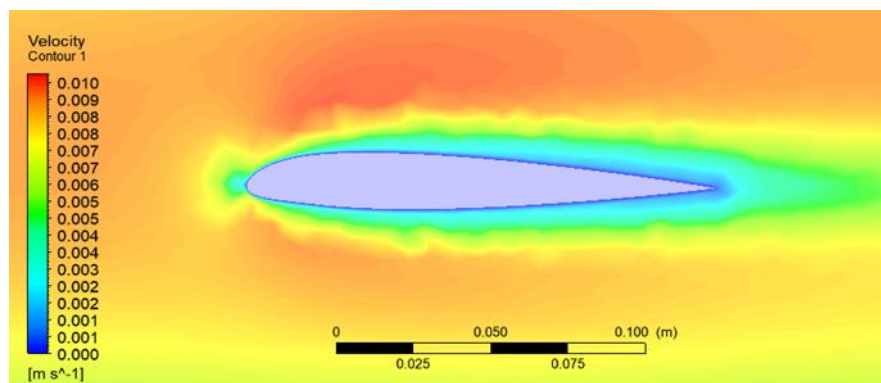


**Fig. 30.** Velocity contour of an airfoil by computer-aided-simulation

### 3.2.4 Flow around car model

Figure 31 and Figure 32 show the comparison between experimental flow visualisation and computer-aided simulation around the car model. In these figures, turbulent flow occurs in the area behind the car. This is in line with the previous study [25]. As shown in Figure 33, the flow on the car's surface decreased in speed, which is indicated in blue, resulting in a boundary layer effect.

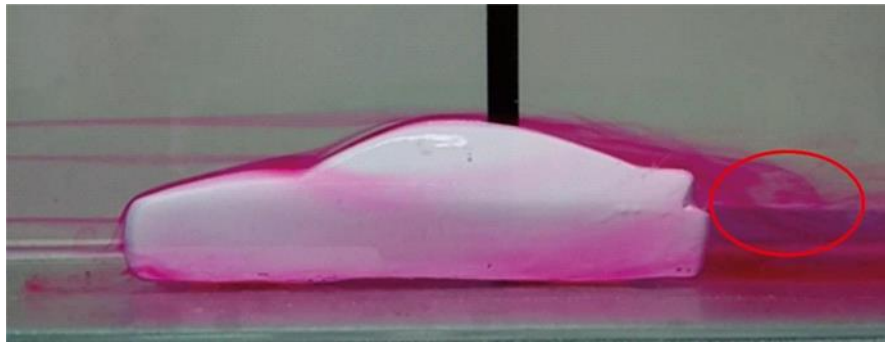


**Fig. 31.** Experimental flow visualization of car model

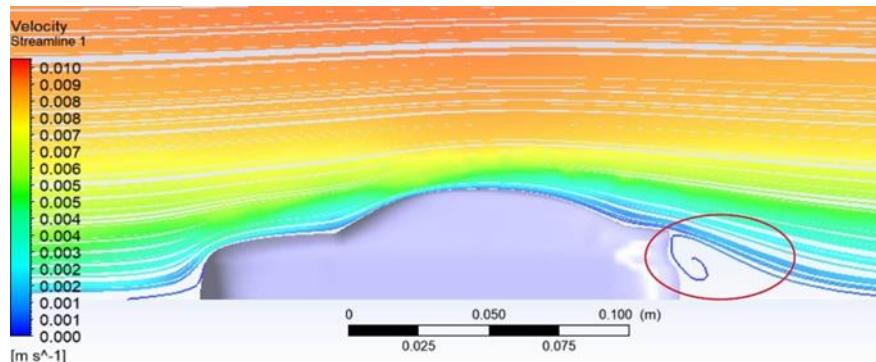


**Fig. 32.** Velocity streamline of a car model by computer-aided simulation

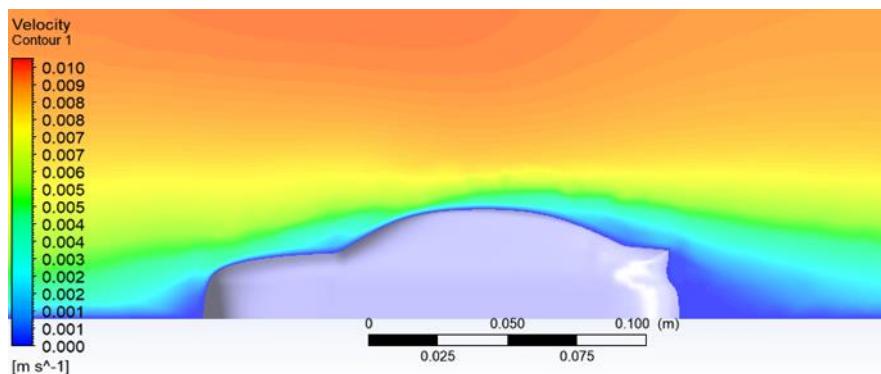


**Fig. 33.** Velocity contour of a car model by computer-aided-simulation

#### 4. Conclusions

Based on the results of the analysis of the experimental and computer-aided simulation, it was found that the addition of diffuser vanes to a wide-angle diffuser can provide a significant change in flow streamlines. The flow velocity achieved in the working section is 0.008 m/s and the flow is laminar. The twelve diffuser vanes could be very effective in minimizing turbulent flow and could provide stable flow in this low-speed water tunnel design. Comparison between the experimental flow visualization and computer-aided simulation provided a flow pattern that is almost similar to every object.

#### Acknowledgement

This research was not funded by any grant.

## References

- [1] Ali, Jaffar Syed Mohamed, Mohd Farid Amran, and Nurul Aziz Mohamad. "Experimental Study on the Effect of Boundary Layer Control on the Aerodynamics Characteristics of NACA 0021 Aerofoil." *Journal of Advanced Research in Fluid Mechanics and Thermal Sciences* 94, no. 1 (2022): 129-137. <https://doi.org/10.37934/arfmts.94.1.129137>
- [2] Ramli, Muhammad Ridzwan, Wan Mazlina Wan Mohamed, Hamid Yusoff, Mohd Azmi Ismail, Ahmed Awaludeen Mansor, Azmi Hussin, and Aliff Farhan Mohd Yamin. "The Aerodynamic Characteristics Investigation on NACA 0012 Airfoil with Owl's Wing Serrations for Future Air Vehicle." *Journal of Advanced Research in Fluid Mechanics and Thermal Sciences* 102, no. 1 (2023): 171-183. <https://doi.org/10.37934/arfmts.102.1.171183>
- [3] Baker, Esam Abu Baker Ali Abu, Iskandar Shah Ishak, Tholudin Mat Lazim, Mohamed Mohamed Takeyeldin, and Abul Bashar Mohammad Abu Haider. "Aerodynamic Performance Investigation of a Small Horizontal Axis Wind Turbine with Multi-Airfoil Blade Profiles of SD2030 and E231 Using Wind Tunnel Experiments and BEM Theory Method." *Journal of Advanced Research in Fluid Mechanics and Thermal Sciences* 103, no. 1 (2023): 150-164. <https://doi.org/10.37934/arfmts.103.1.150164>
- [4] Adrian, Ronald J. "Particle-imaging techniques for experimental fluid mechanics." *Annual review of fluid mechanics* 23, no. 1 (1991): 261-304. <https://doi.org/10.1146/annurev.fl.23.010191.001401>
- [5] Brücker, Ch. "3D scanning PIV applied to an air flow in a motored engine using digital high-speed video." *Measurement Science and Technology* 8, no. 12 (1997): 1480. <https://doi.org/10.1088/0957-0233/8/12/011>
- [6] Wong, Kok-Hoe, Weldon Lai, Jing-Hong Ng, Ahmad Fazlizan, Kamaruzzaman Sopian, and Niranjana Sahoo. "Open-Loop Subsonic Suction Type Wind Tunnel: Design, Simulation, Build and Test:-." *Journal of Advanced Research in Fluid Mechanics and Thermal Sciences* 105, no. 2 (2023): 204-223. <https://doi.org/10.37934/arfmts.105.2.204223>
- [7] P. M. Gerhart and R. J. Gross, *Fundamentals of Fluid Mechanics*. Massachusetts: Addison-Wesley Publishing Company, 1985.
- [8] Çengel, Yunus A., Robert H. Turner, John M. Cimbala, and Mehmet Kanoglu. *Fundamentals of thermal-fluid sciences*. Vol. 703. New York: McGraw-Hill, 2001.
- [9] Zahari, M., and S. S. Dol. "Design and development of low-cost water tunnel for educational purpose." In *IOP Conference Series: Materials Science and Engineering*, vol. 78, no. 1, p. 012040. IOP Publishing, 2015. <https://doi.org/10.1088/1757-899X/78/1/012040>
- [10] Boelens, Okko Joost. "CFD analysis of the flow around the X-31 aircraft at high angle of attack." *Aerospace Science and Technology* 20, no. 1 (2012): 38-51. <https://doi.org/10.1016/j.ast.2012.03.003>
- [11] Sargison, Jane E., Andrew F. Barton, G. J. Walker, and P. A. Brandner. "Design and calibration of a water tunnel for skin friction research." *Australian Journal of Mechanical Engineering* 7, no. 2 (2009): 111-124. <https://doi.org/10.1080/14484846.2009.11464585>
- [12] Kalgutkar, Sanket V., Shubham K. Khobragade, Kishor U. Masurkar, Sayalee Sawant, Vivek Tople, and Shruti Wasnik. "Design, Fabrication and Analysis of Low Speed Water Tunnel."
- [13] Faisal, Safaa H. "Design, fabrication, and testing of heat conduction apparatuses at a low cost." *International Journal of Mechanical Engineering Education* 51, no. 2 (2023): 89-110. <https://doi.org/10.1177/03064190231153101>
- [14] Nedyalkov, Ivaylo. "Design of Contraction, Test Section, and Diffuser for a High-Speed Water Tunnel." (2012).
- [15] Kalyankar, Harshad, Rishabh Melwanki, Dinesh Choudhary, Siddharth Jethwa, and Dipak Chaudhari. "Design and analysis of low speed water tunnel for flow visualization of bluff body." In *2nd Int. Conf. Adv. Mech. Eng. Its Interdiscip. Areas*, pp. 49-57. 2015.
- [16] Loehrke, R. I., and H. M. Nagib. "Control of free-stream turbulence by means of honeycombs: a balance between suppression and generation." (1976): 342-351. <https://doi.org/10.1115/1.3448313>
- [17] Nguyen, Quoc Y. "Designing, constructing, and testing a low-speed open-jet wind tunnel." *International Journal of Engineering Research and Applications* 4, no. 1 (2014): 243-246.
- [18] Meng, Xu, Zhigang Zuo, Michihiro Nishi, and Shuhong Liu. "A numerical study on the flow mechanism of performance improvement of a wide-angle diffuser by inserting a short splitter vane." *Processes* 8, no. 2 (2020): 143. <https://doi.org/10.3390/pr8020143>
- [19] Arifuzzaman, Mohammad, and Mohammad Mashud. "Design construction and performance test of a low cost subsonic wind tunnel." *IOSR Journal of Engineering* 2, no. 10 (2012): 83-92. <https://doi.org/10.9790/3021-021058392>
- [20] Anderson, John David, and John Wendt. *Computational fluid dynamics*. Vol. 206. New York: McGraw-hill, 1995.
- [21] Saha, S., and B. Majumdar. "Flow visualization and CFD simulation on 65 delta wing at subsonic condition." *Procedia engineering* 38 (2012): 3086-3096. <https://doi.org/10.1016/j.proeng.2012.06.359>
- [22] Daneshi, Mojtaba. "Numerical investigation of the fluid flow around and past a circular cylinder by ANSYS simulation." *Int. J. Adv. Sci. Technol* 92 (2016): 49-58. <https://doi.org/10.14257/ijast.2016.92.06>

- [23] Yagmur, Sercan, Sercan Dogan, Muharrem Hilmi Aksoy, Ilker Goktepli, and Muammer Ozgoren. "Comparison of flow characteristics around an equilateral triangular cylinder via PIV and Large Eddy Simulation methods." *Flow Measurement and Instrumentation* 55 (2017): 23-36. <https://doi.org/10.1016/j.flowmeasinst.2017.04.001>
- [24] Supreeth, R., A. Arokkiaswamy, K. Anirudh, R. K. Pradyumna, P. K. Pramod, and A. K. Sanarahamat. "Experimental and numerical investigation of the influence of leading edge tubercles on S823 airfoil behavior." *Journal of Applied Fluid Mechanics* 13, no. 6 (2020): 1885-1899. <https://doi.org/10.47176/jafm.13.06.31244>
- [25] Banga, Saurabh, Md Zunaid, Naushad Ahmad Ansari, Sagar Sharma, and Rohit Singh Dungriyal. "CFD simulation of flow around external vehicle: Ahmed body." *IOSR Journal of Mechanical and Civil Engineering* 12, no. 4 (2015): 87-94. <https://doi.org/10.9790/1684-1204038794>